EFFECTS OF SPANWISE BLOWING ON PRESSURE DISTRIBUTION AND LEADING-EDGE VORTEX STABILITY

ICAS-86-2.5.1

J. Er-El and A. Seginer
Department of Aeronautical Engineering
Technion - Israel Institute of Technology
Haifa 32000, Israel

Abstract

Spanwise-blowing (SWB) effects on the leading-edge vortex trajectory and breakdown and on the pressure distribution over a 60 deg delta wing/ogive-cylinder body configuration was investigated experimentally in low speed flow. Schlieren pictures through a transparent wing were recorded in addition to pressure mapping. Flow visualization showed that the interaction of the SWB jets with the surrounding flow and its effects on the vortex stability greatly depended on the proximity of the SWB nozzles to the vortical core of the vortices. Mounting a body over the wing resulted in an increase in the leading-edge suction peak and in its outward displacement, while decreasing the suction over the inboard part of the wing. The overall lift remained equal to that of the wing alone in the linear-lift range of the angle of attack, fell below that of the wing in the nonlinear-lift range, and delayed the wing stall at $\alpha>30$ deg by stabilizing the vortex. SWB also increased the suction peak and decreased the suction over the inboard parts of the wing at the lower angles of attack ($\alpha\leq 20$ deg). At higher angles the effect on the suction peak was decreasing and acting over a narrowing area in the apex region, but the suction over the inboard wing was increasing, so that the overall effect was a fairly constant lift increment in the angle-of-attack range of $\alpha\leq 25$ deg. At higher angles of attack SWB delayed the vortex breakdown and greatly enhanced the lift of the configuration.

I. Introduction

Leading edge vortices, whether generated by the highly-swept leading edge itself or by a special inboard part of the wing (such as on double-delta wings, straked wings or close-coupled-canard configurations) are widely used on modern fighter aircraft to produce additional (so called "nonlinear" or "vortex") lift[1]. The utilization of the vortex lift is limited by the vortex-breakdown phenomenon (VBD) that occurs at higher angles of attack[2].

Although the exact nature of the VBD and its causes are still in dispute[3] its delay by blowing along the vortex core, or "spanwise blowing" (SWB) has been well established[4]. The overall effects of SWB were first investigated over a flat plate[5], over a flap[6] and over a wing[7]. The investigation was then extended to many wing planforms and configurations (e.g. Refs. 4, and 8 through 11).

The results of the above-mentioned work were mostly of an integral nature, such as the overall effect of SWB on the lift or drag. Data on the details of the interaction of the blown jets with the vortices were scant indeed, and could not shed light on the nature of the interaction.

A second shortcoming of existing data on SWB was a discrepancy between data from several sources. Whereas most researchers reported that SWB on highly swept wings (such as the 60 deg delta) only increased the maximum lift by delaying VBD[10,11], Ref. 12 reported a significant lift augmentation throughout the angle-of-attack envelope. It is interesting to note that a similar discrepancy was found also in the canard effects on the performance of a 60 deg delta wing. When tested over a wing alone the canard, although it did stabilize the vortex, did not add to the lift of the wing itself[13] and its contribution to the overall lift of the configuration was significant at angles of attack above 26 deg only[14]. On the fighter configuration of Ref. 12, however, the contribution of the canard was significant throughout the angle-of-attack envelope.

As both SWB and the canard enhance the lift by stabilizing the vortex and delaying VBD one must wonder if the two discrepancies described above are not the result of a common cause. The main differences between the wing-alone and fighter-configuration tests were that in the latter case the canard and SWB were interacting with a wing that was mounted below a fuselage and that also had a conically drooping leading edge. To investigate the reason for these discrepancies one would have to repeat the SWB tests over the basic wing model, but with a fuselage mounted over it.

The main objective of this work was to add detailed information on the mechanism of SWB. This was done by visualizing the effect of SWB on the trajectory and breakdown of the vortex and by measuring the signature of SWB on the pressure distribution over the wing. A secondary objective was to get some better insight on the influence that the body has on SWB.

Flow visualization was done using a transparent wing in conjuncture with a sensitive schlieren system. These tests were carried out on a wing alone because a fuselage would have obstructed the passage of the light rays. Consequently, the results of the flow visualization are of a more general character on the influence of SWB on the vortex trajectory and breakdown and cannot shed light on the above-mentioned discrepancy. Pressure distributions, on the other hand, were mapped over a wing-body configuration to emphasize the body effects. In both the flow-visualization tests and the pressure mappings the wing was a simple flat plate with a sharp leading edge. This was done to separate the possible effects of the body and the drooping leading edge. The

effects of a leading-edge droop will be investigated at a later stage.

II. Experimental Apparatus and Program

The wind-tunnel tests were conducted on two models and in two wind tunnels. The pressure distributions were measured in the 1mx1m cross-section, low-speed (30 m/s) wind tunnel on a lower-wing/fuselage model (Fig. 1a) that was a modification of the model of Refs. 13, 15 and 16. The wing was a sharp-edged, flat-plate, 60 deg-sweep delta with a root chord of C_r=0.246 m and a uniform thickness of 0.0046 m, and with symmetrical wedge-shaped edges of 30 deg vertex angle. An cone-cylinder body with a 0.037 m diameter and slenderness ratio of 13.67 (the cone was 4.16 diameters long) was mounted on the wing to simulate the aircraft configuration of Ref. 12. The nose of the body was 5.62 diameters upstream of the wing apex in order to reduce the nose effects on the wing.

Air was blown from the fuselage at a total pressure of 6 at. At this pressure the jet-momentum coefficient C_μ, which is the product of the jet mass flux and its exit velocity normalized by the freestream dynamic pressure and the wing-planform area, was equal to C_μ=0.18. The blowing was parallel with the leading edge from two nozzles, of 2.6 mm inner diameter, located 0.015 C_r above the wing surface and 0.04 C_r inboard from the leading edge. The positions of the SWB nozzles were the same as those that were found to be optimal on the aircraft configuration of Ref. 12. Because the body in the present work differed from the fuselage of the aircraft model, two additional nozzle locations also were tested. One was at the same height above the wing but further aft (0.02 C_r), and the other was 0.02 C_r higher and slightly aft from the nominal position. Both of these locations were found to be less effective than the nominal one.

One hundred and twenty-five pressure taps, of 0.6 mm inner diameter were drilled into the upper surface of the wing along ten rays that emanated from the apex (Fig. 1b). The taps were located on fourteen rows, parallel with the trailing edge, with ten taps to the row, except for the first three rows that had six taps in the first row and seven each in the second and third rows (Fig. 1b). When the fuselage was mounted on the wing it covered several of the inboard pressure taps, neutralizing them (Fig. 1b).

The pressure measurement system consisted of three 48 ports Scanivalve SGM modules, each connected to a Type 6 or Type 96 Statham pressure transducer. The model was pitched to discrete angles of attack (nominally from zero to 35 deg, at intervals of 5 deg) and at each angle of attack the pressures were scanned, reduced to pressure coefficients and recorded. The pressures were integrated to give local (chordwise or spanwise) and overall normal-force coefficients. The pressures on the lower surface of the wing, that were needed for these integrations were obtained from Ref. 17, assuming that the effects of either upper body or SWB on the pressure distribution over the lower surface of the wing were negligible[18].

The flow-visualization tests were conducted on a modified version of the transparent-wing model of Ref. 14 in the induction-type 60 cm x 80 cm cross-section, transonic wind tunnel at a Mach number of M=0.3. The wing was a flat, 60 deg sweep delta wing with a sharp, bevelled leading edge (Fig. 2). Two stainless-steel tubes of 0.16 mm inner diameter were led along the root chord of the lower surface of the wing, and through the wing in the apex area, where they were bent parallel with the leading edge. The nozzle axes on this model were at the same nominal locations as the nozzles on the pressure model. However, as the flow visualization tests were conducted without a fuselage, it was doubtful if this location was optimal on the wing-alone model too. Two additional nozzle positions were, therefore, tested on this model. In the one marked as Configuration II the nozzles axes were 0.015 C_r above the nominal position, and in the second (Configuration III) the axes were approximately 0.025 C_r downstream of the nominal position. As expected, the nominal nozzle position (Configuration I) was indeed not optimal[19].

The vortex core and breakdown were visualized using a sensitive schlieren system. SWB was done with helium (results of blowing also with air are reported in Ref. 19). The blowing of a gas with a distinctly different density from that of the surrounding air made the jets visible in the schlieren photographs.

III. Results and Discussion

Visualization Tests

Typical examples of side views of the flow field with and without SWB are presented in Figs. 3a through 3d. Figure 3a, that shows SWB at zero angle of attack, is brought as a reference. At $\alpha=0^\circ$ the SWB jets interact with the freestream only and are not affected by the leading-edge vortices that develop at higher angles of attack. Another reference is the wing at α=15 deg without SWB (Fig. 3b) that shows clearly the vortex breakdown.

When the SWB is turned on its effect depends on the nozzle location. When the jet is injected close to the vortex axis (Fig. 3c) it stabilizes the vortex and VBD is delayed to a further outboard and downstream position. When helium is used, as in this case, the injected gas seems to mix with the vortex and the helium/air mixture in the vortex enhances the visualization of the vortex core and its axis. On the other hand when the helium is injected at some distance from the vortex core it is less effective in delaying VBD (Fig. 3d) and its seems to mix with the air outside, or on, the periphery of the rotational core, obscuring (by its different density) the vortex axis. The seemingly mixing of the jet with the vortex is in contradiction with the observations of Ref. 20 and others, and will have to be further investigated.

Some explanation of this discrepancy maybe found in the top views of the flow field in Figs. 4a, 4b and 4c. Figure 4a shows the trajectory of the jets at α=0 deg, when they are swept downstream by the freestream only with no vortex

effects. At $\alpha \simeq 15$ deg (Fig. 4b) a vortex has been formed near the leading edge but it is apparently too weak to affect the jet, except to displace it slightly inward. When the angle of attack is increased to $\alpha \simeq 22$ deg (Fig. 4c) the vortex is both wider and stronger and the jet is bent strongly toward the vortex. The detail in the photograph is insufficient to decide if the jet material is ingested into the vortex or wraped around it. However, the latter seems to be more likely, and also explains the obscuring of the vortex by the nelium.

Pressure Distributions

The effects of the body on the flow over the wing are evaluated by a comparison of the pressure distributions over the exposed parts of the wing (in the wing/body configuration) with the distributions over the wing alone (as obtained from Refs. 13, 16, 17). A second comparison of the pressure distribution over the exposed parts of the wing, in the same wing/body model but this time with SWB, with the distributions without SWB isolates the effects of SWB.

Body Effects. The pressure distributions over the exposed parts of the wing with the body mounted on it are compared in Figs. 5a through 5e with those over the wing alone, at angles of attack of α=15,20,25,30 and 35 deg, C_p in these figures is the pressure coefficient, $\bar{y}$ is the local dimensionless spanwise position and $\bar{x}$ is the dimensionless chordwise position.

Generally speaking, one can see that the body displaces the suction peak outward and increases the peak, especially over the fore two thirds of the wing (chord positions 38% and 65%). As the angle of attack is increased the pressures over the inboard parts of the wing also increase due to the presence of the body (the absolute value of the pressure coefficient, C_p, is decreasing). This should mean loss of lift due to the body as the angle of attack is increasing. On the other hand, the body has a stabilizing effect on the leading-edge vortices. At α=25 deg one can already see the symptoms of VBD over the wing alone in the relative flatness of the pressure distributions[13] near the trailing edge (Fig. 5c). When the body is present these distributions display the suction peak that characterizes a vortex. This effect is more pronounced at α=30 deg (Fig. 5d) and is quite dramatic at α=35 deg (Fig. 5e) where the pressure over the wing alone is practically constant, indicating the existence of VBD and massive separation, whereas the body generates some additional suction near the leading edge. This indicates that VBD is delayed by the body and that an increase in lift, relative to the wing alone, should be expected at the higher angles of attack.

In drawing these conclusions one must remember though that the body effect, described above, maybe either the result of the outward displacement of the flow field by the body, or a stabilization of the wing vortices by vortices that maybe shed from the nose of the body at these angles of attack. This point needs further investigation.

Similarity Between Wing-Alone and Wing/Body. In analysing the body effects on the pressure distribution one must bear in mind the fact that the distributions that are compared in Fig. 5 were measured at the same physical points on the wing. The relative axial and spanwise positions of these points on the exposed (or wetted) parts of the wing differ from those of the wing alone. To ensure that this difference is not the only reason for the differences between the pressure distributions, the distributions of the wing/body model were replotted after spanwise and chordwise interpolation to the correct relative positions (Figs. 6a, 6b, 6c). At α=15 deg the distributions over the two models (Fig. 6a) are fairly similar, except for a small increase in the suction peaks over the aft 20% of the wing. At α=25 deg (Fig. 6b) there is a relative narrowing of the high-suction region, with the increase in the suction peak spreading upstream also to the 2/3 chord position. Over the aft third of the chord the wing-alone distributions are characteristic of VBD whereas the body effect is clearly stabilizing the vortices. This is even more pronounced at α=35 deg (Fig. 6c). These results indicate that at the lower angles of attack, where the vortices are weak, both cases are fairly similar. At the high angles of attack, when the vortices become dominant, the body is affecting the vortices in a nonsimilar manner.

SWB Effects. These effects can be evaluated from the comparison of the pressure distributions over the wing/body model with, and without, SWB (Figs. 7a through 7e). Generally speaking again SWB increases the suction peak, but at the same time, also narrows it and moves it outward. This results in higher suction over the outboard parts of the wing, but also in higher pressures over the inboard parts. The overall effect on the lift cannot, therefore, be evaluated outright from these figures.

At α=15 deg (Fig. 7a) this effect is observed over the whole wing. At α=20 deg (Fig. 7b) it is decreasing, except for the apex region. At the 65% chord position no increase in the suction peak is observed. At α=25 deg the increase in the suction peak and the outward shift in its location are now limited to the apex region (Fig. 7c). The diminishing effect of SWB is shown in Fig. 7d for α=30 deg. Except for the apex region, the suction peak is now reduced by SWB over the aft part of the wing, but this loss is offset by lower pressures over the inboard part of this region.

SWB effects pick up again at α=35 deg where the vortices over the wing alone are nonexistent, but partially revitalized by the body effects (Fig. 5e). In this case with SWB (Fig. 7e) the pressure distributions show, again, the signature of the leading-edge vortices with a distinct suction peak.

Normal-Force Coefficient

The pressure distributions, discussed above, presented local effects only, whereas the integral body, or SWB effects were hard to evaluate. Consequently, these distributions were integrated (together with the corresponding distributions over the lower surface of the wing from Ref. 17) to furnish the normal-force coefficient, C_N.

The angle-of-attack dependence of C_N is presented for the various test configurations in Fig. 8.

The nonlinear vortex lift of the wing alone (circles) is evdident at α>15 deg, as is also the stall because of VBD at α=35 deg. The normal-force coefficient of the wing/body configuration (triangles) follows that of the wing alone for $\alpha \leq 15$ deg and then falls below it. This indicates that, although the body seems to stabilize the wing vortices, it also causes lift loss by raising the pressures over the inboard parts of the wing (Figs. 5b, 5c, 5d). However, when the wing alone finally stalls (α=35 deg) the vortices, that are partially stabilized by the body, generate sufficient lift to prevent stalling of the wing/body configuration, although the beginning of lift saturation is already indicated (Fig. 8). The same result is obtained both when the pressures are integrated over the exposed parts of the wing only and the normal-force coefficient is normalized by their area only (solid inverted triangles), and when the integration and normalization are done using the whole wing area. In the latter case it is assumed that the pressure over the central part of the wing that is covered by the body is constant and equal to that measured at the wing-body junction. This validates the lift-carry-over assumption that is often used in wing/body lift prediction[21].

SWB increases the normal-force coefficient over the whole angle-of-attack range (compared with the wing/body data in Fig. 8). The slope of the lift curve with SWB is only slightly larger than that with blowing off, up to α=25 deg. This could mean that most of the normal-force increment in this range is directly contributed by the low static pressure that is locally induced by the jets and their interaction with the main flow field. It is only at α>25 deg, when the wing/body contribution approaches lift saturation, that SWB really comes into its own by stabilizing the vortices and by maintaining the same lift curve slope.

IV. Conclusions

The effects of SWB on the trajectories and breakdown of the leading-edge vortices and on the pressure distribution over a 60 deg delta-wing/ogive-cylinder-body model were investigated experimentally in low-speed flow. Body effects on the wing were obtained as a by-product because the blowing was done from nozzles in the body.

The flow visualization tests, using a schlieren system with a transparent wing and blowing helium, showed that the interaction of the SWB jets with the surrounding flow in general, and with the vortices in particular, depends strongly on the proximity of the SWB nozzles to the vortical core of the vortices. At close proximity the jet stabilizes the vortex and the jet material seems to be ingested into the core flow. As the distance between the vortex core and jet increases, the SWB stabilizing effect decreases and the jet material seems to envelope the core by swirling around it.

When a body is mounted over an existing wing it displaces the suction peak outward, closer to the leading edge, and in most cases increases the suction peak while reducing the suction over the inboard parts of the wing. The integral effect of the body is that in the linear-lift range the wing and wing/body configurations generate the same lift. In the nonlinear-lift range the body reduces the lift of the wing by reducing the wing area under the suction peak. At still higher angles of attack the body delays the stall by stabilizing the wing vortices.

Spanwise blowing increases the suction peak, but at the same time also narrows its width and increases the pressures over the inboard parts of the wing. These SWB effects are felt over a decreasing area, narrowing down to the apex region, as the angle of attack increases, but these diminishing effects are offset by lower pressures over the inboard part of the wing, so that the lift increment due to SWB is fairly constant up to α=25 deg. Lift augmentation by SWB becomes very significant at α>25 deg when VBD is delayed by SWB and the vortex lift continues to increase, at least up to α=35 deg.

To conclude, SWB increases the lift over a 60 deg delta wing, as a lower wing in a wing/body configuration, throughout the angle-of-attack range up to α=35 deg. Its most significant contribution is at α>25 deg when the wing/body configuration without SWB approaches lift saturation.

References

1. Kuchemann, D., "On the Possibility of Designing Wings that Combine Vortex Flows with Classical Airfoil Flows", RAE Tech. Memo., Aero. 1363, Oct. 1971.

2. Wentz, W.H., Jr. and Kohlman, D.L., "Wind Tunnel Investigation of Vortex Breakdown on Slender Sharp-Edged Wings", NASA CR-98737, 1969.

3. Leibovich, S., "Vortex Stability and Breakdown", Paper No. 23 in "Aerodynamics of Vortical Type Flows in Three Dimension", AGARD-CP-342, April 1983.

4. Staudacher, W., Laschka, B., Poisson-Quinton, P., and Ledy, J.P., "Effects of Spanwise Blowing in the Angle-of-Attack Regime α=0-90°", Proceedings of the 11th Congress of ICAS, Vol. 1, Sept. 1978, pp. 89-95.

5. Dixon, C.J., "Lift Augmentation by Lateral Blowing Over a Lifting Surface", AIAA Paper 69-193, AIAA/AHS VTOL Research, Design and Operations Meeting, Feb. 1969.

6. Cornish, J.J., III, "High Lift Applications of Spanwise Blowing", ICAS Paper No. 70-09, 7th Congress of ICAS, Rome, Italy, Sept. 1970.

7. Poisson-Quinton, P., "Controle du D'ecollment D'use Surface Portante par un Jet Transversal", Intervention au 7 iem Congress ICAS, Rome, Italy, 1970.

8. Clarke, K.P., "Lift Augmentation on a Moderately Swept Wing by Spanwise Blowing", Aeronautical Journal, Vol. 80, Oct. 1976, pp. 447-451.

9. Erickson, G.E., "Effects of Spanwise Blowing on the Aerodynamic Characteristics of a Half-Span 50° Swept Cropped Delta Wing Configuration", AIAA Paper 79-1859, AIAA Aircraft Systems and Technology Meeting, New York, N.Y. Aug. 1979.

10. Bradley, R.G. and Wray, W.O., "A Conceptual Study of Leading-Edge-Vortex Enhancement by Blowing", Journal of Aircraft, Vol. 11, Jan. 1974, pp. 33-38.

11. Campbell, J.F., "Augmentation of Vortex Lift by Spanwise Blowing", Journal of Aircraft, Vol. 13, Sept. 1976, pp. 727-732.

12. Seginer, A. and Salomon, M., "Augmentation of Fighter Aircraft Performance by Spanwise Blowing Over the Wing Leading Edge", AGARD CP-342, Paper No. 33, April 1983, also NASA TM 84330, March 1983.

13. Er-El, J., "The Effect of Wing/Canard Interference on the Loading of the Delta Wing", Accepted for publication in the Journal of Aircraft.

14. Er-El, J. and Seginer, A., "Vortex Trajectories and Breakdown on Wing-Canard Configurations", Journal of Aircraft, Vol. 22, Aug. 1985, pp. 641-648.

15. Er-El, J. and Zohar, Y., "An Experimental Examination of the Leading-Edge Suction Analogy", Accepted for publication in the Journal of Aircraft.

16. Zohar, Y. and Er-El, J., "The Influence of the Aspect Ratio on the Aerodynamics of the Delta Wing at High Angles of Attack", Submitted for publication in the Journal of Aircraft.

17. Zohar, Y., "The Effects of Vortex Breakdown on the Aerodynamic Properties of Delta Wings", M.Sc. Thesis, Technion-I.I.T., Haifa, Israel, 1984.

18. Campbell, J.F. and Erickson, G.E., "Effects of Spanwise Blowing on the Surface Pressure Distributions and Vortex-Lift Characteristics of a Trapezoidal Wing-Strake Configuration", NASA TP 1290, Feb. 1979.

19. Er-El, J., "The Visualization of the Flow Field About a Delta Wing with Spanwise Blowing", Submitted for publication in Experiments in Fluids.

20. Dixon, C.J., "The Mechanism of Vortex Control by Spanwise Blowing and Wing Geometry", Lockheed Georgia Co., Mariett, GA., Engineering Report LG78-ER-0187, June 1978.

21. Rusak, Z., Wasserstrom, E. and Seginer, A., "Numerical Calculation of Nonlinear Aerodynamics of Wing-Body Configurations", AIAA Journal, Vol. 21, July 1983, pp. 929-936.

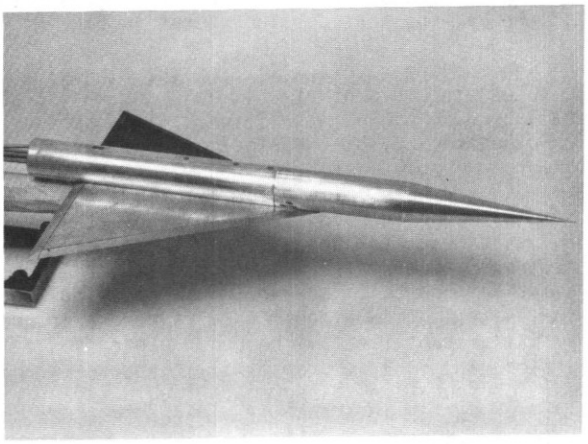

(a) Overall view.

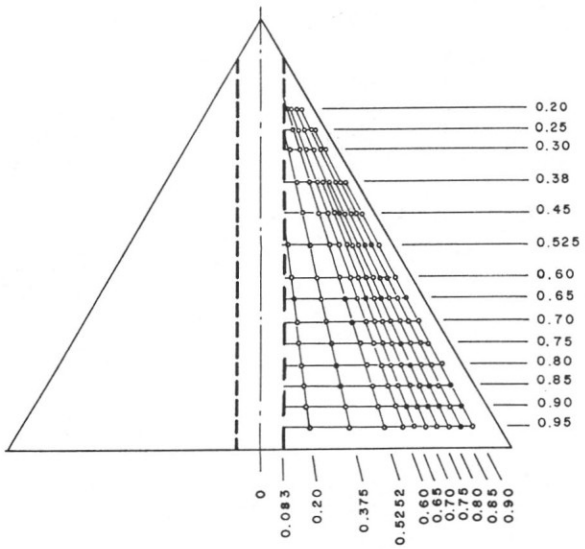

(b) Map of the pressure holes on the wing. The region between the dashed line is enclosed in the body.

Fig. 1. The pressures model with body overlay.

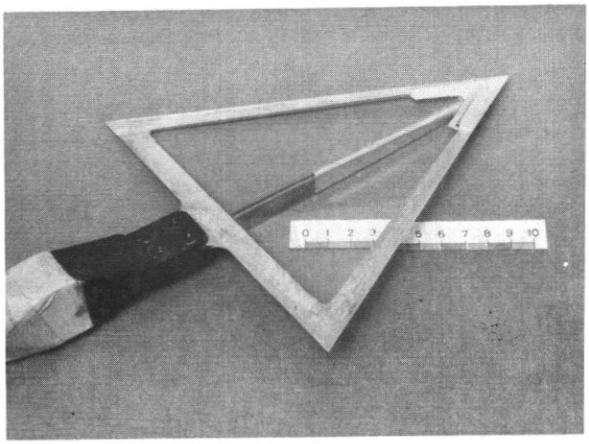

Fig. 2. The transparent wing.

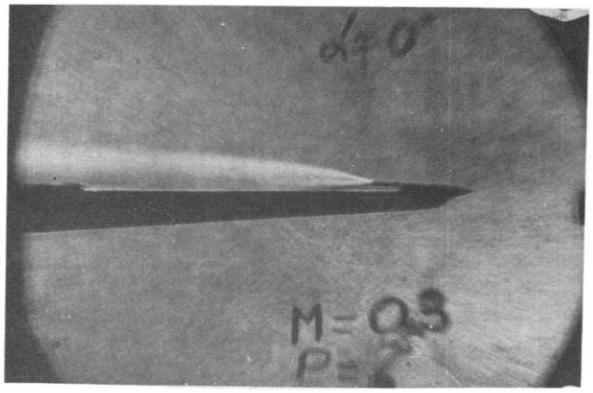

(a) $\alpha=0^\circ$, $C_\mu=0.02$, Conf. II.

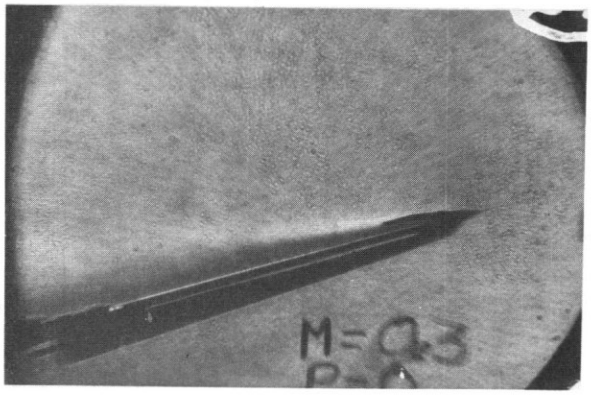

(b) $\alpha\simeq15^\circ$, $C_\mu\simeq0$.

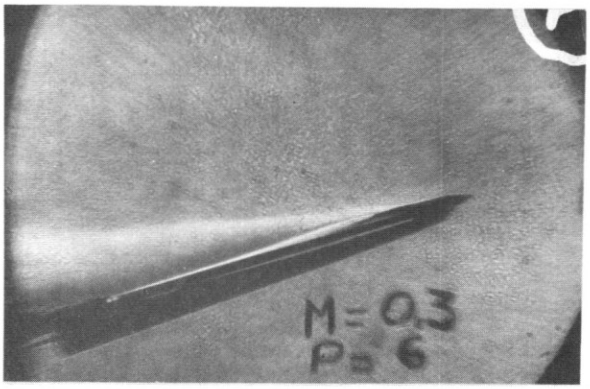

(c) $\alpha\simeq15^\circ$, $C_\mu=0.02$, Conf. II.

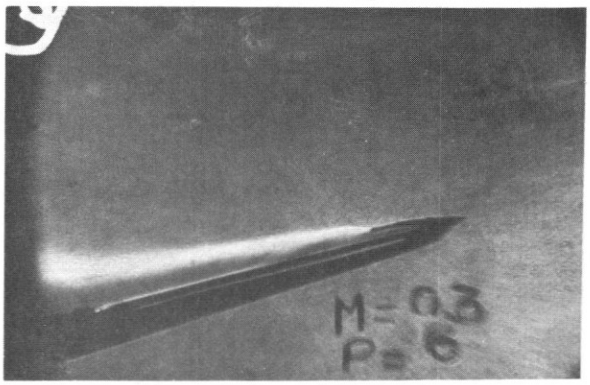

(d) $\alpha\simeq15^\circ$, $C_\mu=0.02$, Conf. III.

Fig. 3. Side views of SWB with helium.

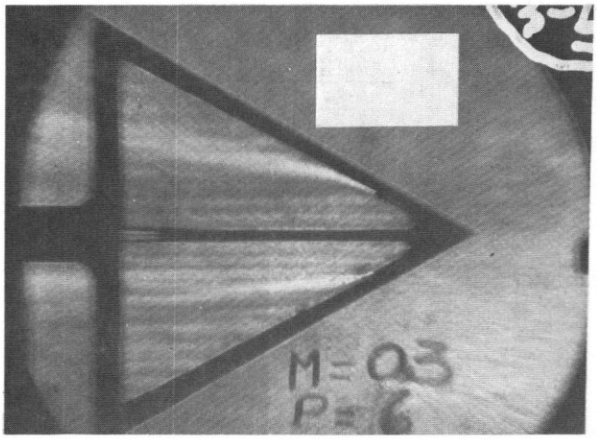

(a) $\alpha=0^\circ$.

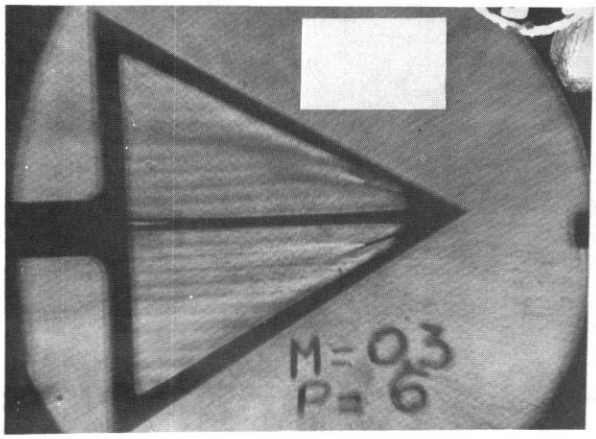

(b) $\alpha\simeq15^\circ$, $C_\mu=0.02$, Conf. II.

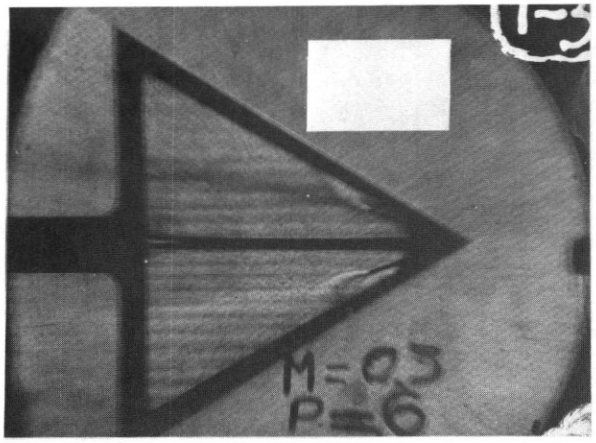

(c) $\alpha\simeq22^\circ$, $C_\mu=0.02$, Conf. II.

Fig. 4. Top views of SWB with helium.

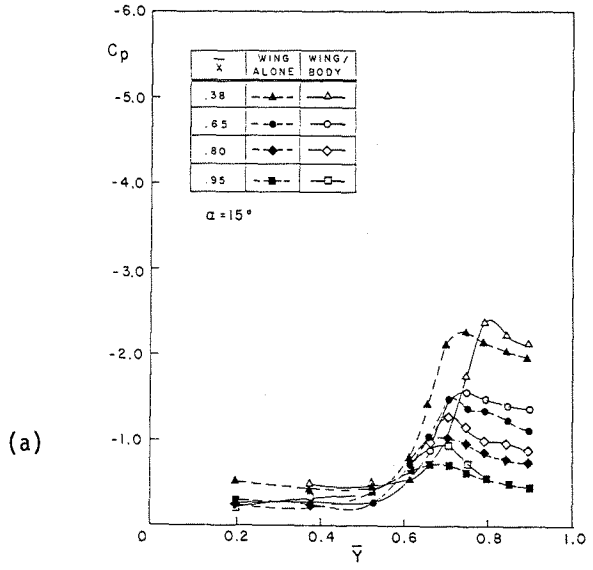

(a)

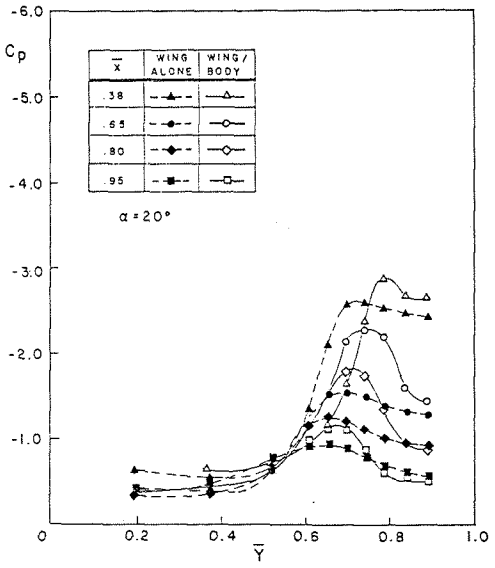

(b)

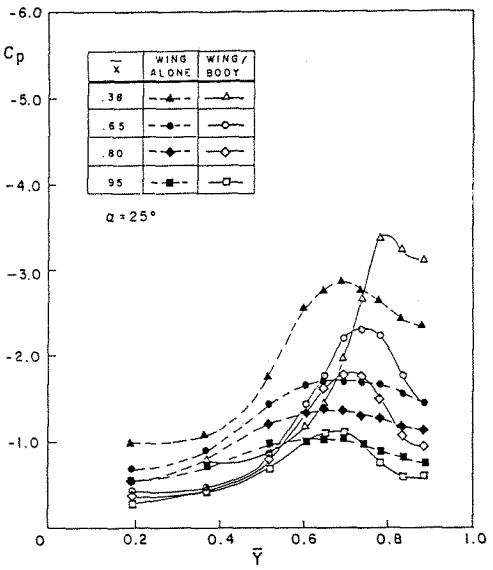

(c)

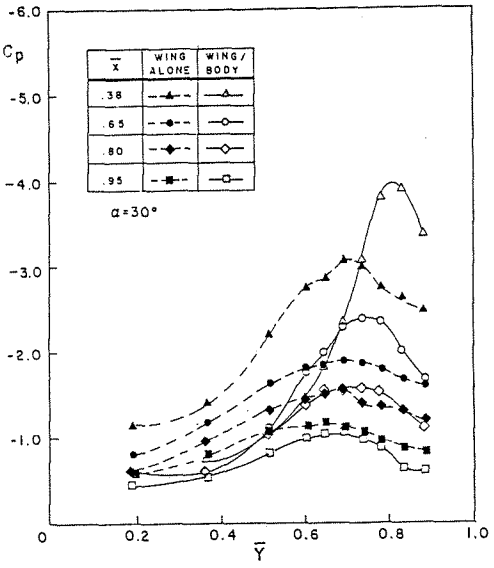

(d)

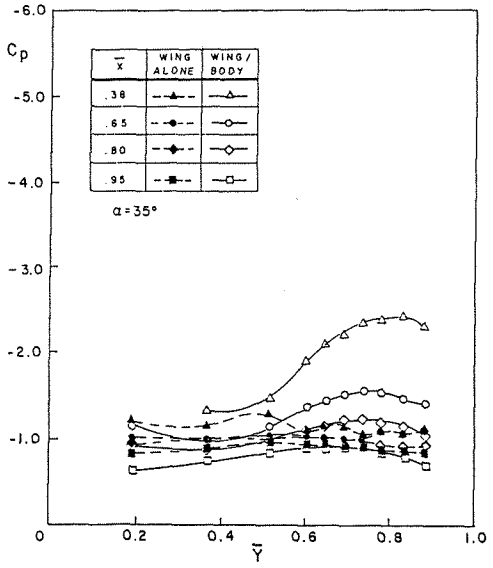

(e)

Fig. 5. Body effects on the pressure distributions.

(a) $\alpha=15^{\circ}$.
(b) $\alpha=20^{\circ}$.
(c) $\alpha=25^{\circ}$.
(d) $\alpha=30^{\circ}$.
(e) $\alpha=35^{\circ}$.

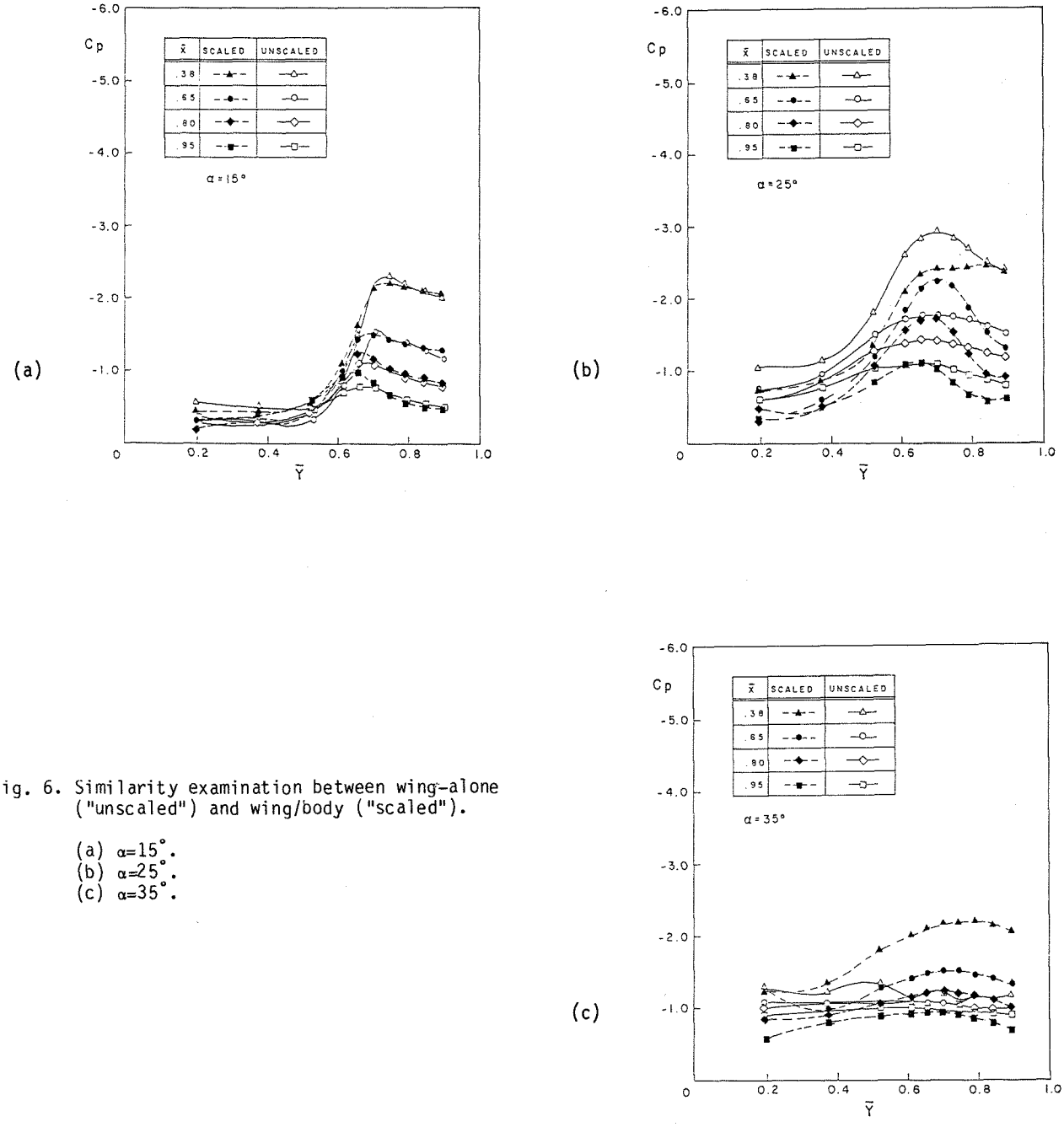

Fig. 6. Similarity examination between wing-alone ("unscaled") and wing/body ("scaled").

(a) $\alpha=15^{\circ}$.
(b) $\alpha=25^{\circ}$.
(c) $\alpha=35^{\circ}$.

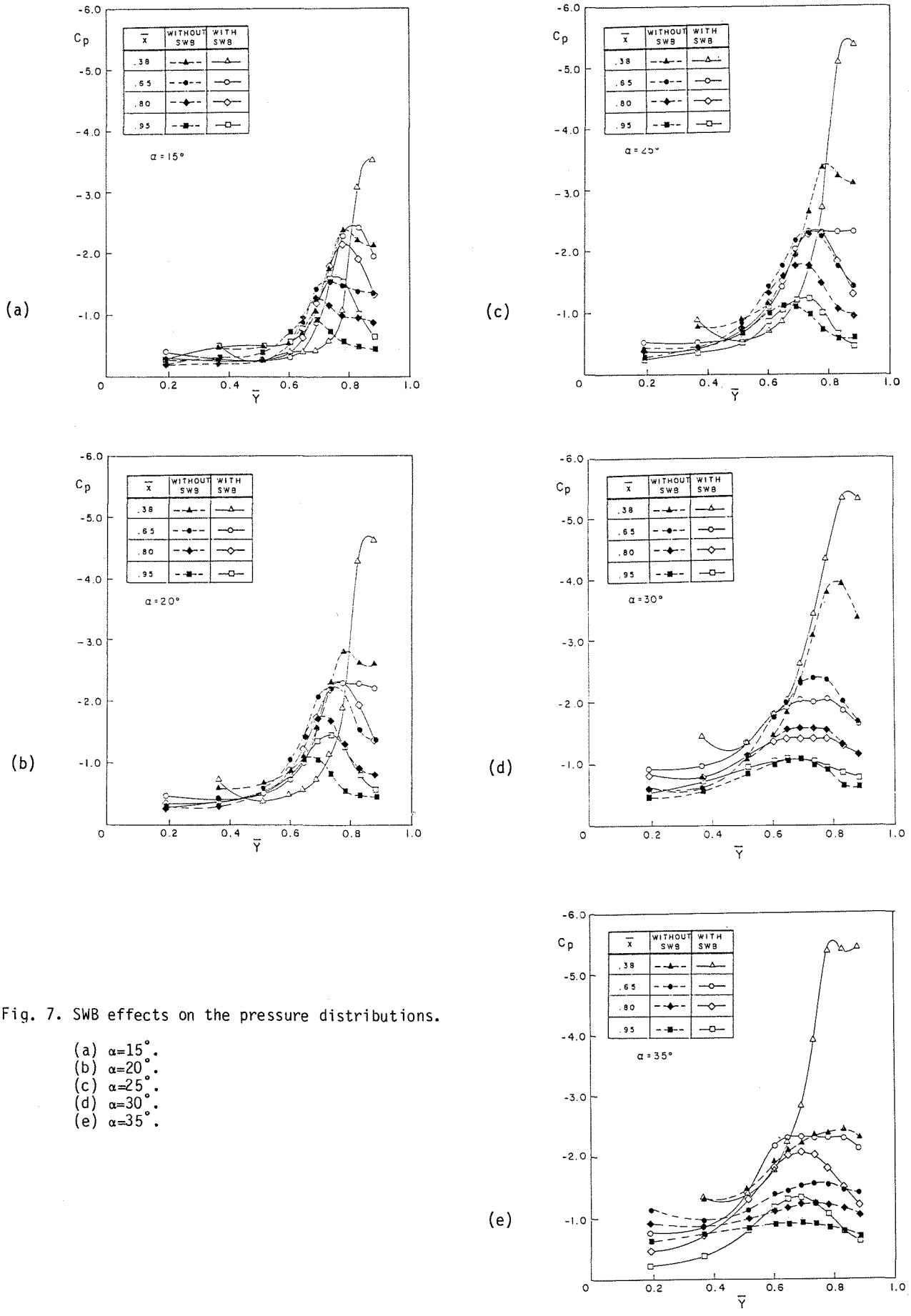

Fig. 7. SWB effects on the pressure distributions.

(a) α=15°.
(b) α=20°.
(c) α=25°.
(d) α=30°.
(e) α=35°.

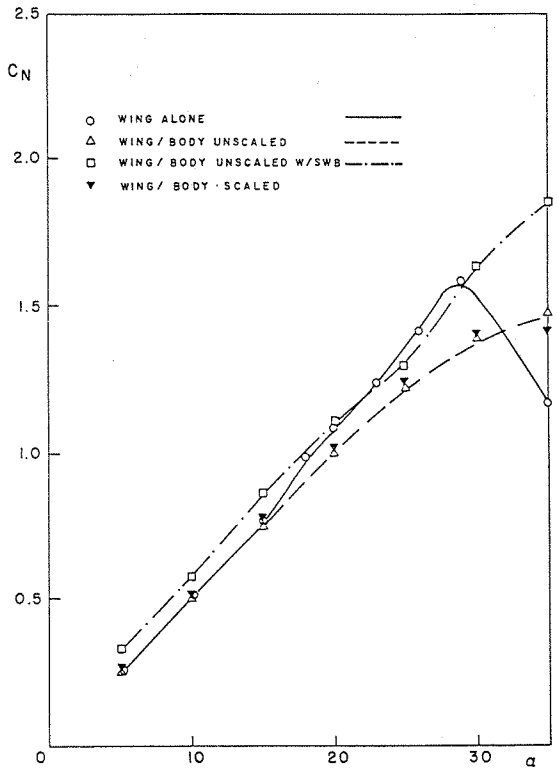

Fig. 8. Normal-force coefficient.